Natural Convection in a Vertical Open-Ended Channel: Comparison between Experimental and Numerical Results

Amine Zoubir, Christophe Daverat, Shihe Xin, Stéphanie Giroux-Julien, Hervé Pabiou, Christophe Menezo

Journal of Energy and Power Engineering 7 (2013) 1265-1276

Natural Convection in a Vertical Open-Ended Channel: Comparison between Experimental and Numerical Results

Zoubir Amine[1, 2], Christophe Daverat[1, 2], Shihe Xin[1, 2], Stéphanie Giroux-Julien[1, 3], Hervé Pabiou[1, 2] and Christophe Ménézo[1, 4]

1. University of Lyon, Centre National de la Recherche Scientifique, France

2. Institut National des Sciences Appliquées de Lyon, CETHIL UMR5008, F-69621, Villeurbanne, France

3. Université Lyon 1, CETHIL UMR5008, F-69621, Villeurbanne, France

4. Chair Institut National des Sciences Appliquées de Lyon/Electricité de France "Energy Innovations and Habitats", CETHIL UMR5008, F-69621, Villeurbanne, France

Received: September 19, 2012 / Accepted: December 11, 2012 / Published: July 31, 2013.

Abstract: The present study deals with natural convection flow in a vertical open-ended channel with wall constant heat flux. The experimental and numerical investigations are both conducted using water as the working fluid. The numerical code is developed using finite differences scheme to solve the Navier-Stokes equations under the Boussinesq assumption. Concerning the experimental apparatus, it consists of two heated walls immersed in water. Temperature and velocity measurements are provided for different modified Rayleigh numbers based on the walls spacing b $Ra^{*}_{b} = 1.67 \times 10^{6}, 3.6 \times 10^{6}, 8.97 \times 10^{6}, 1.69 \times 10^{7}, 4.29 \times 10^{7}$. The numerical code is first validated with a numerical benchmark. Then, comparison between experimental and numerical results is performed. The code provides a satisfactory prediction of main quantities compared to the experimental results but only for the lowest Rayleigh numbers. For higher modified Rayleigh numbers, the flow becomes three-dimensional and turbulent. Therefore, 2D numerical simulations fail to predict flow and heat transfer for this range of modified Rayleigh number.

Key words: Natural convection, vertical channel, numerical study, experimental study.

1. Introduction

The working temperature of BIPV (building integrated photovoltaic) components is a key factor in terms of efficiency. The configurations for integration of these components can cause an increase in operating temperature and a decrease of their electrical efficiency. In order to cool them by natural convection, they are mounted in a double-skin configuration, meaning that they are separated from the building envelope by an open-ended air gap. Identifying and analyzing the physical phenomena that govern the air flow and fluid/wall heat transfer in this vertical channel are therefore essential to improve photovoltaic panel cooling. This can only be performed by detailed numerical simulations validated by experimental studies. Many authors have worked on natural convection in vertical channels. Author in Ref. [1] was the first, who worked on natural convection between two 12 × 12 cm^2 isothermal parallel plates for cooling electronic components. He underlined that convective heat transfer is characterized by Nusselt, Grashof and Prandtl numbers and presented a correlation giving the Nusselt number as a function of the modified Rayleigh number. The model of heat transfer was assumed 2D and covered a range of modified Rayleigh numbers of

Corresponding author: Zoubir Amine, Ph.D., research fields: natural convection heat transfer, fluid mechanics. E-mail: amine.zoubir@insa-lyon.fr.

$Ra_b^* < 10^5$ (Eq. (4)) and pure conductive flow regimes. Bodoia et al. [2] presented the first numerical simulation on natural convection in a 2D isothermal vertical channel. The results were compared with those in Ref. [1] and showed quite good agreement except for low Rayleigh numbers. This discrepancy was attributed to side leakage effects in experimental apparatus in Ref. [1]. Moreover, they characterized two asymptotic regimes for laminar convective flows in vertical channels. At low Rayleigh numbers, the asymptotic regime corresponds to the analytical solution given in Ref. [3]. For high Rayleigh numbers it tends towards the free convective flow along a vertical flat plate that is described by the theoretical solutions in Ref. [4]. Aung et al. [5-7] conducted a series of numerical approaches using the boundary layer approximation. The common feature of these studies is the so-called parabolic approach. Actually, this approach gives satisfactory results at moderate modified Rayleigh numbers but fails to predict the flow behavior at higher values. It has to be noticed that such computations require imposing an inlet velocity profile. The interesting results of this set of works resides in the fact that heat transfer does not depend on the choice of entry velocity profile as long as Ra_b^* is sufficiently small (flow in developed regime). This has been pointed out in Ref. [8].

Several attempts have equally been performed for solving the full set of Boussinesq [9-11]. Investigations also came up against the problem of inlet dynamical boundary conditions. In order to overcome this intrinsic difficulty the way usually chosen is to defer fixing the entry boundary conditions. In the same way, Kettleborough, et al. [9-11] added a large extension to the channel entry in order to fix inlet conditions at some more distant entry. The additional computational effort implied in this way is a source of severe limitations on efficiency. Practically, numerical contributions are limited to $Ra_b^* < 300$ and $A < 12$, where A is the ratio between the height and the width of the channel. Ramanathan et al. [12] studied free convection in a channel immersed within a large enclosure. This approach is unfortunately very expensive in computing time. Consequently, it yields relatively poor agreements with experimental data obtained in Ref. [13], especially at high modified Rayleigh number. In addition, a correction on the pre-heating of the incoming air at the inlet is required because its temperature is higher than the initial inlet temperature. From a numerical point of view the main difference with most open flows is the fact that flow driving force (i.e., the buoyancy) is within the computational domain and therefore inlet flow can not be prescribed, neither in terms of intensity nor in terms of profile. In this way, the thermally driven channel acts as a thermal engine. Its behavior would in fact depend on the external mechanical resistance and on free space thermal stratification (if stratification occurs). It is then interesting to close the Boussinesq equations with inlet/outlet boundary conditions in order to approach at best what happens outside the channel in experiments.

The present study deals with a comparison between numerical and experimental results on natural convection between two heated walls with uniform and symmetrical fluxes for large aspect ratio $A \approx 14.5$ and large modified Rayleigh numbers $Ra_b^* = 1.67\times10^6, 3.6\times10^6, 8.97\times10^6, 1.69\times10^7, 4.29\times10^7$. For this range of parameter we expect that one can focus the modeling on the channel itself [14]. On the other hand, if the channel aspect ratio is less than 10 and Ra_b^* is too small, we can not do without one of the methods quoted above [9-11].

In a double-skin facade configuration, the thermal boundary conditions at the walls are close to uniform non-symmetric fluxes, but in this study we consider symmetric and uniform heated walls in order to qualify the numerical results in comparison with reference experimental ones. Both numerical and experimental studies are conducted using water as the working fluid in order to get rid of radiation heat transfer and to have a pure convective flow. In fact, we need to characterize first the pure natural convection flow in the channel in

order to identify the physical mechanisms that drive both the convective heat transfer and chimney effect before including the radiation heat transfer. Although many experimental and numerical studies on natural convection between parallel plates have been carried out [15-23], most studies were limited to thermal measurements and heat transfer analysis. Few studies were interested in the flow dynamics quantities [16, 19, 20]. However, these dynamic quantities are needed to qualify numerical simulations with the experimental measurements. In addition, most of studies have been done using air as working fluid and the radiation part of heat transfer is still not completely known [24-26]. In order to contribute in the understanding of the physical mechanisms of natural convection, we present both experimental and numerical investigations of thermal and dynamic quantities for pure convective flow (with water). Furthermore, as the authors work with high Rayleigh numbers and large aspect ratio, the computational domain was truncated in order to reduce the computational time.

In the following, the experimental model including the design and the characterization of the apparatus is introduced first. Secondly, the authors describe the physical model and the numerical study. Algorithms for solving temperature and pressure-velocity coupling are briefly clarified. Numerical methods are then validated by comparing numerical results with GDR-AMETH benchmark [27] that addresses the problem of natural convection of air (without surfaces radiation) between two vertical walls, one wall is isolated and the other one is heated with uniform heat flux. Finally, a comparison between experimental data and numerical results is made on main quantities.

2. Experimental Apparatus

This part describes the experimental apparatus set up for studying natural convection in a vertical water channel.

2.1 Design

The apparatus shown in Fig. 1 is a vertical channel of

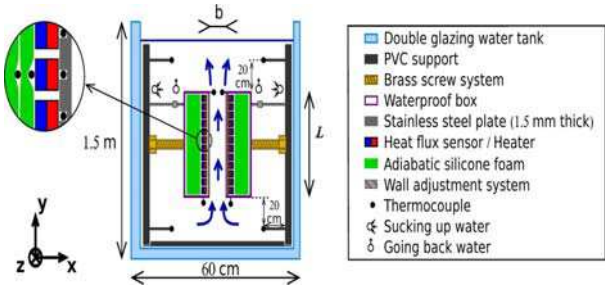

Fig. 1 Cross section in the xOy plane showing the different parts and sensors of the experimental apparatus. The dimension ratios are not represented faithfully in this drawing.

internal dimensions $b \times 65 \times 23.5$ cm^3 (in directions x, y and z) positioned in a water tank. Y is the ascending vertical and the width b is adjustable. The vertical channel is formed by two waterproof boxes which contain electrical heaters and is closed on the lateral edges by the double-glazing walls of the water tank. Each box is maintained by a brass screw fastening system that is fixed to a Polyvinylchloride board (Fig. 1). The heated part is 61.1 cm high and the gap between walls is b = 45.1 mm. The boundary conditions in the channel are isoflux conditions on the heated walls (stainless steel plates) and adiabatic conditions on the lateral walls (glass tank walls). Each stainless steel plate is heated by 12 electrical resistances supplied with a constant current. It is important to notice that the stainless steel plate which dimensions are 65 × 23.5 cm^2 are heated over a surface of 61.1 × 20 cm^2 located at its center. To limit heat conduction between the heated part of the plate and the upstream and downstream parts, 1 mm deep grooves are machined in the plate right next the first and last heaters. The water temperature is regulated by a thermo-regulation system.

2.2 Characterization

Velocity measurements are performed in the channel with a LDV (laser Doppler velocimetry) system mounted on a motorized 2D-translation stage allowing velocity measurements along y and x in the channel mid-plane. The mean velocity profiles are obtained averaging during 25-30 min for each point. Temperature is measured by thermocouples. All measurements in the channel are performed under

steady-state conditions. The operating conditions are assumed to be steady when the evolution of the temperature in the tank (top, bottom, channel inlet and outlet) was weak, and when the top, bottom and channel outlet temperatures did not change compared to the channel inlet temperature. Fig. 2 presents the temperature evolutions at the top and bottom of the tank, at the channel inlet and outlet and in the room (thermocouple positions are shown in Fig. 1) during experiment 4 (Table 1). Depending on the experimental conditions, statistically steady-state regime is generally reached after 24-48 h. The temperature of the water in the tank is assumed to be homogenous when the difference between the tank top and channel inlet temperatures is almost null. The second controlled boundary condition is the uniform isoflux condition on the channel walls. It is presented in Fig. 3 by plotting the mean wall heat flux on each heater versus the dimensionless channel height during experiment 5 (Table 1). It shows that a uniform isoflux condition is reached with mean variations lower than 1%. On the other hand the maximum fluctuations measured are lower than 2% (not shown in this figure). Moreover, the difference between the mean heat flux on the left and right walls is lower than 0.01%. Thus uniform symmetrical isoflux condition can be assumed on the channel walls.

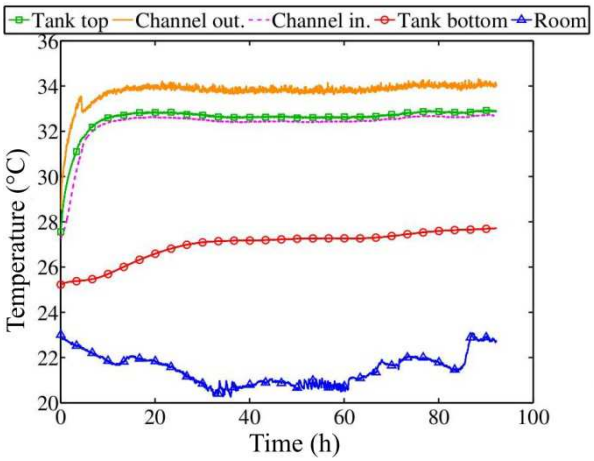

Fig. 2 Temperature evolutions in the tank (and room) during experiment 4 (Table 1).

Table 1 The five experimental studied configurations. Wall heat flux is the value averaged over the two walls and over time. Inlet and tank top temperatures are time averaged values.

Experiment	Uniform heat flux(W/m^2)	Temperatures °C		Ra_b^*
		Inlet	Top tank	
1	190	22.58	22.62	1.67×10^6
2	382	23.45	23.48	3.6×10^6
3	764	27.31	27.36	8.97×10^6
4	1,147	32.56	32.60	1.69×10^7
5	2,305	36.54	36.58	4.29×10^7

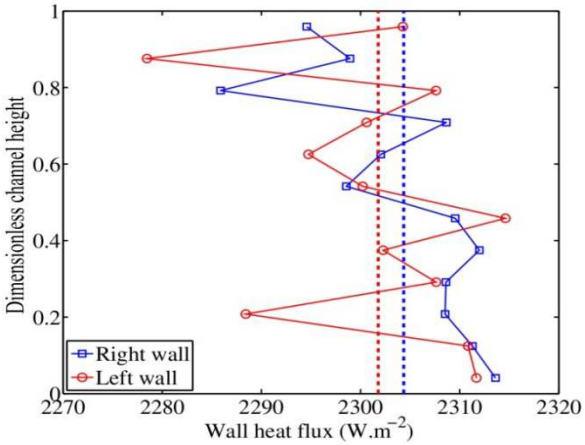

Fig. 3 Time average heat flux on channel walls (square: right, circle: left) versus dimensionless channel height during experiment 5 (Table 1).

3. Physical Model and Numerical Study

3.1 Numerical Modeling

Two geometrical configurations subject to investigation are shown in Figs. 4 and 5. Fig. 4 corresponds to the air flow benchmark of GDR-AMETH laboratories [27] used for the numerical methods validation. Fig. 5 concerns the simplified (2D) configuration of the experimental apparatus. The wall heating produces a temperature gradient in the fluid leading to small density differences which gives rise to the buoyancy force. Thus, a natural convective flow occurs with the fluid entering at the bottom and leaving at the top. Throughout the analysis the following assumptions are made: fluid properties, except density, are independent of temperature; density variations are significant only in the buoyancy force; and the flow is two-dimensional, laminar and incompressible with negligible viscous dissipation. Thus, the well-know

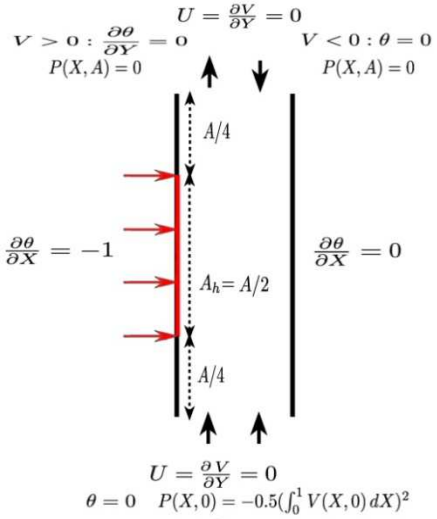

Fig. 4 Benchmark configuration with boundary conditions. The channel is submitted to asymmetrical heating at fixed flux.

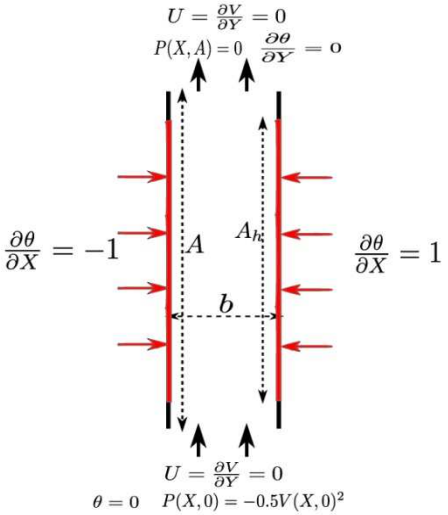

Fig. 5 Experimental configuration with boundary conditions. The channel is submitted to symmetrical heating at fixed flux.

unsteady Boussinesq equations in their elliptic form, governing the flow, are:

$$\begin{cases} \dfrac{\partial u}{\partial x}+\dfrac{\partial v}{\partial y}=0 \\ \dfrac{\partial u}{\partial t}+u\dfrac{\partial u}{\partial x}+v\dfrac{\partial u}{\partial y}=-\dfrac{1}{\rho_0}\dfrac{\partial p}{\partial x}+\nu_0\left(\dfrac{\partial^2 u}{\partial x^2}+\dfrac{\partial^2 u}{\partial y^2}\right) \\ \dfrac{\partial v}{\partial t}+u\dfrac{\partial v}{\partial x}+v\dfrac{\partial v}{\partial y}=-\dfrac{1}{\rho_0}\dfrac{\partial p}{\partial y}+\nu_0\left(\dfrac{\partial^2 v}{\partial x^2}+\dfrac{\partial^2 v}{\partial y^2}\right)+g\beta_0(T-T_0) \\ \dfrac{\partial T}{\partial t}+u\dfrac{\partial T}{\partial x}+v\dfrac{\partial T}{\partial y}=\alpha_0\left(\dfrac{\partial^2 T}{\partial x^2}+\dfrac{\partial^2 T}{\partial y^2}\right) \end{cases} \quad (1)$$

where, u, v, p are respectively, horizontal velocity, vertical velocity and pressure. $\rho_0, \nu_0, \beta_0, \alpha_0$ are respectively, mass density, kinematic viscosity, thermal expansion coefficient and thermal diffusivity calculated at some reference temperature T_0. By introducing the following non-dimensional quantities with reference variables (L_r, U_r, t_r):

$$L_r = b, \quad X = \frac{x}{L_r}, \quad Y = \frac{y}{L_r}, \quad U_r = \sqrt{\frac{\beta_0 g \Delta T b}{\mathrm{Pr}}},$$

$$U = \frac{u}{U_r}, \quad V = \frac{v}{U_r}, \quad \theta = \frac{T-T_0}{\Delta T}, \quad P = \frac{p-p_0}{\rho_0 U_r^2},$$

$$t_r = \frac{b}{U_r}$$

The governing equations are transformed as follows:

$$\begin{cases} \dfrac{\partial U}{\partial X}+\dfrac{\partial V}{\partial Y}=0 \\ \dfrac{\partial U}{\partial t}+U\dfrac{\partial U}{\partial X}+V\dfrac{\partial U}{\partial Y}=-\dfrac{\partial P}{\partial X}+\mathrm{Pr}Ra_b^{-1/2}\left(\dfrac{\partial^2 U}{\partial X^2}+\dfrac{\partial^2 U}{\partial Y^2}\right) \\ \dfrac{\partial V}{\partial t}+U\dfrac{\partial V}{\partial X}+V\dfrac{\partial V}{\partial Y}=-\dfrac{\partial P}{\partial Y}+\mathrm{Pr}Ra_b^{-1/2}\left(\dfrac{\partial^2 V}{\partial X^2}+\dfrac{\partial^2 V}{\partial Y^2}\right)+\mathrm{Pr}\theta \\ \dfrac{\partial \theta}{\partial t}+U\dfrac{\partial \theta}{\partial X}+V\dfrac{\partial \theta}{\partial Y}=Ra_b^{-1/2}\left(\dfrac{\partial^2 \theta}{\partial X^2}+\dfrac{\partial^2 \theta}{\partial Y^2}\right) \end{cases} \quad (2)$$

where ΔT used to define the non-dimensional temperature and the reference velocity is: $\Delta T = \dfrac{q_w b}{\lambda_0}$, in which q_w is the uniform heat flux fixed at the wall. The Prandtl number Pr is defined by: $Pr = \nu_0/\lambda_0$. Furthermore, the Rayleigh number, expressing the strength of buoyancy, is constructed with the plate spacing as follows:

$$Ra_b = \frac{g\beta_0 q_w b^4}{\nu_0 \alpha_0 \lambda_0} \quad (3)$$

This finally leads to Ra_b^*, the modified Rayleigh number (or Elenbaas number):

$$Ra_b^* = \frac{Ra_b}{A_h} \quad (4)$$

where $A_h = \dfrac{L_h}{b}$ is the aspect ratio of the heated part of the channel (Figs. 4 and 5).

The selected boundary conditions for the thermally driven open channel are shown in Figs. 4 and 5. When the boundary conditions are expressed in pressure at the inlet, the generalized Bernoulli theorem is used to take into account the pressure loss between the upstream and the entry of the channel (upstream velocity assumed to be zero and the pressure is equal to $p(x, y = 0) = p_{atm}$). Indeed, Dalbert, Morrone, Marcondes, et al. [7, 17, 28] found that the driving pressure at the entrance of the channel, due to the velocity of the incoming fluid, can not be neglected, the influence is even more important as the Rayleigh number increases. Local Bernoulli pressure is applied at the channel entrance (Fig. 5). Moreover, pressure at the outlet is taken equal to exterior pressure assumed to be zero (atmospheric pressure in dimensional form). When boundary conditions are written on velocity, zero Neumann boundary condition is applied on streamwise velocity V and homogeneous Dirichlet boundary condition is applied on transverse velocity U. Actually, the authors assume that the incoming flow at the inlet is parallel to the channel. Same kinematic boundary conditions are used for the benchmark configuration except for pressure at the channel inlet. Global Bernoulli was used instead of local Bernoulli. Global Bernoulli seems to overestimate the flow rate at the channel inlet [27]. The authors therefore test the local Bernoulli in the case of comparison with experimental data. Concerning the thermal boundary conditions, the authors neglect the longitudinal conductive heat flux at the channel outlet, knowing that the transverse thermal gradients are more important. If in some case, an incoming flow can appear at the channel outlet, the authors assume it has the outside temperature. In this approximation, the authors neglect the fact that the incoming fluid may be slightly heated in the external surroundings.

The next part of this section deals with numerical methods used to discretize the Boussinesq equations with finite difference schemes in time and space. Algorithms for solving temperature and pressure-velocity coupling are detailed.

3.2 Numerical Methods

Equations of conservation of mass, momentum, and energy, are discretized with finite differences schemes in space and time. The temporal scheme adopted to discretize the system of Eq. (2) is based on the three-level second-order Euler backward scheme with Adams-Bashforth extrapolation as proposed in Ref. [29]. In this scheme, the authors treat implicitly the diffusion terms and explicitly the convective ones. The pressure velocity decoupling is achieved by adopting an iterative solution based on a projection algorithm [30, 31]. This algorithm consists of finding first a velocity prediction based on pressure field approximation. Then an equation for pressure correction is derived from the continuity equation, it is then solved to obtain the pressure correction to update the velocity fields and pressure. Concerning the spatial discretization, the computational domain is discretized on a non-uniform Cartesian grid. Use is made of a staggered variable arrangement. A second order centered difference schemes are used for all variables. A second order forward and backward difference schemes are used to treat the Neumann boundary condition on vertical velocity respectively at the inlet and at the outlet.

After discretization, the authors obtain a Poisson equation on pressure correction and Helmholtz equations on velocity and temperature. The authors solve the Poisson and Helmholtz equations respectively using partial diagonalization method and tridiagonal matrix algorithm. For more details see Ref. [32].

4. Validation

4.1 Comparison with GDR-AMETH

The thermally driven vertical channel problem has served as a benchmark problem. The GDR AMETH laboratories [27] have worked on natural convection of air between two vertical walls, one heated by a uniform heat flux and the other insulated (Fig. 4). This kind of problems leads to a so-called flow reversal when

channel walls are subjected to asymmetric heating [16, 33, 34]. In this benchmark, four dynamic boundary conditions are tested in order to approach the Webb and Hill experimentation [25]. The purpose of this section is not to qualify the open boundary conditions used in this benchmark, but, to validate our numerical code by comparing characteristic quantities. The comparison is made for modified Rayleigh number of $Ra_b^* = 10^5$ and aspect ratio of $A = 10$ and different grid resolutions. Numerical results are furnished in Table 2. One can notice that our numerical results are in very good agreement with all the other works. The discrepancy is less than 2% on characteristic quantities except with results of the LIMSI laboratory for which the discrepancy reaches 5% on velocity.

4.2 Grid Convergence Analysis

In order to assess the quality of numerical solution and to quantify its spatial accuracy, the authors calculated the order of accuracy on the temperature and the normal component of velocity using the grid convergence error analysis described in Refs. [35-38]. Numerical simulations were conducted for very long time in order to reach the steady state regime and to minimize the residual error. Consider the values of variable f computed on a coarse grid (f_C), a medium grid (f_M), and a fine grid (f_F). The corresponding grid sizes are respectively $\Delta x_C = 0.016, \Delta x_M = 0.008, \Delta x_F = 0.004$. The ratio $R = \dfrac{f_C - f_M}{f_M - f_F} = 2^p$ has been used to categorize the behavior of f as grid is refined, where the exponent p is the spatial scheme order. Estimations of (f_M) and (f_F) on the coarse grid were obtained by a fourth-order interpolation. In this study, a modified Rayleigh number of $Ra_b^* = 100$ and a channel aspect ratio of $A = 5$ are used. Table 3 shows some local values of vertical velocity and temperature at different points. The ratio R takes a value about 4 in most points and this means that the spatial numerical scheme is globally of second order (p = 2). Furthermore, some points take a ratio slightly less than 4 on temperature (points 6 and 7 in Table 3). These two points are both near the heated and the adiabatic parts of the left wall (Fig. 4). In fact, there is a temperature gradient discontinuity in this area. Certainly, a temperature field has no discontinuities. Nevertheless, discontinuities in the gradient of temperature are rather common and potentially able to change the nominal order of convergence.

5. Comparison between Numerical and Experimental Results

The configuration of interest is a water-filled vertical channel and the corresponding natural convection flow is studied both experimentally and numerically. The boundary conditions on the heated walls were isoflux

Table 2 Comparison of average and local Nusselt numbers, average velocities and maximum inlet/outlet velocity with GDR-AMETH laboratories results.

$Ra_b = 5\times10^5$, $A_h = A/2 = 5$								
	80 × 800	100 × 1,000	150 × 900	150 × 1,500	200 × 1,200	TREFLE	MSME	LIMSI
$\overline{Nu}$	6.948	6.945	6.937	6.937	6.936	6.98	6.92	6.95
$Nu_{3A/8}$	7.298	7.295	7.292	7.294	7.286	7.27	7.29	7.30
$Nu_{A/2}$	6.245	6.244	6.237	6.240	6.237	6.22	6.24	6.25
$Nu_{5A/8}$	5.698	5.697	5.693	5.696	5.693	5.68	5.69	5.70
$Nu_{3A/4}$	5.654	5.658	5.661	5.662	5.664	5.53	5.67	5.68
$Nu_{7A/8}$	9.870	9.883	9.872	9.884	9.890	9.88	9.89	9.93
Nu_A	11.928	11.945	11.941	11.954	11.900	12.3	11.9	12
$\overline{V_{out}}$	0.1078	0.1093	0.1089	0.1101	0.1100	0.1098	0.1097	0.1152
G_{bf}	0.0266	0.0254	0.0258	0.0247	0.0249	0.0250	0.0247	0.0213
$\max(V_{in})$	0.1621	0.1643	0.1636	0.1653	0.1651	0.1646	0.1643	0.1746
$\max(V_{out})$	0.4930	0.4939	0.4941	0.4949	0.4947	0.4957	0.4954	0.4951

Table 3 Results on grid convergence and error analysis.

Local points	V_C	V_M	V_F	R	θ_C	θ_M	θ_F	R
1	0.2143569	0.2141905	0.2141491	4.02	0.4466186	0.4467585	0.4467932	4.03
2	0.2445082	0.2443621	0.2443258	4.02	0.4307659	0.4309048	0.4309393	4.03
3	0.2722299	0.2721032	0.2720717	4.03	0.4151738	0.4153115	0.4153456	4.03
4	0.2976245	0.2975161	0.2974893	4.03	0.3998710	0.4000071	0.4000409	4.03
5	0.3207926	0.3207016	0.3206791	4.04	0.3848837	0.3850179	0.3850512	4.03
6	0.0653222	0.0650888	0.0650305	4.00	0.6188714	0.6188428	0.6188351	3.73
7	0.0645064	0.0642826	0.0642267	4.00	0.5997491	0.5996107	0.5995754	3.91

conditions and the external channel temperature was regulated to remain within the band of the Boussinesq approximation. Temperature and velocity were measured for five heat fluxes (Table 1). As important fluctuations are observed experimentally on velocity field, the measurements are averaged for duration of 25-30 min for each point. Uncertainties on velocity and temperature measurements are respectively ±2 mm/s and 0.05 °C. Numerical simulations are also performed for the five experimental configurations. CPU time that is necessary to reach converged solutions varies from 4.6 h to 109.5 h respectively for 100 × 800 to 250 × 2,000 grid resolutions (Table 4). Computations are done on Intel Xeon E5520 2.27 GHz processor with 4 GB memory. Numerical simulations led to steady laminar flows. The possible reasons could be the flow loop in the experiment and the boundary conditions and the 2D assumption used in numerical simulations. As the channel is in a confined environment (the water tank), the water lifts up in the channel, is cooled at the tank top and goes back to the entrance passing behind the waterproof boxes. Flow fluctuations may not be damped enough before reentering the channel and could be amplified further. In simulations, the inlet boundary conditions do not introduce perturbations and the 2D assumption may constrain flow from becoming time-dependent.

Despite of the important difference observed on the time behavior, flow rates and local Nusselt numbers (calculated at the channel outlet) are compared between experimental and numerical results (Tables 4 and 5). The experimental flow rate is calculated at the inlet and the outlet by integrating the measured velocity

Table 4 CPU times for different grid resolutions.

$Ra_b^* = 1.67\times10^6, 3.6\times10^6, 8.97\times10^6, 1.69\times10^7, 4.29\times10^7$		
	$\Delta t = 0.01$	$\Delta t = 0.001$
100 × 800	4.6 h	21.7 h
150 × 1,200		34.6 h
200 × 1,600		62.1 h
250 × 2,000		109.5 h

Table 5 Relative differences between numerical and experimental results in terms of Nusselt number and flow rate.

Ra_b^*	Nu	Q_{inlet} (m^2/s)	Q_{outlet} (m^2/s)
1.67×10^6	7%	32%	15%
3.6×10^6	9%	11.5%	11%
8.97×10^6	19%	24%	0.3%
1.69×10^7	33%	7%	19%
4.29×10^7	55%	14%	33.5%

assuming a 2D profile. In fact, the flow is not 2D: the velocity falls close to the front and rear walls of the water tank (along z direction), boundary layers along these walls thicken from the inlet to the outlet, velocity profile along z direction exhibits a maximum at the channel mid-depth x y-plane. Using velocity measurements at the channel outlet overestimates flow rate: this is why $Q_{outlet/\exp}$ is larger than $Q_{inlet/\exp}$ (Table 4). Numerical results are in agreement with $Q_{inlet/\exp}$ for Experiments 2, 4 and 5 but larger for other experiments. In terms of Nusselt number, agreement is better for the first two configurations and discrepancy is important for the three other configurations.

Figs. 6 and 7 show velocity profiles at the channel inlet $(y/L_h = 0.04)$ and outlet $(y/L_h = 0.96)$ in the five experiments compared to numerical simulations. Chimney effect can be seen at the channel

inlet with fluid rising upwards inside the channel. The dynamic boundary layers develop from the inlet to the channel outlet: because of the wall heating fluid flow is accelerated along the walls, two velocity peaks appear next to them and flow at the channel center is slowed down. Velocity at the channel center is not null but reaches a plateau as shown in Fig. 7. Flow rate increases with the wall heat flux. The higher the wall heat flux is, the higher the velocity peaks are. It can be seen from Fig. 6 that numerical profiles overestimate the experimental ones for Experiments 1-2-3 at the inlet. Although flow rates at the inlet agree well between numerical and experimental results for Experiments 4 and 5, the profiles are quite different. At the outlet (Fig. 7), discrepancies are only significant at the channel center for Experiments 1-2 and close to the heated walls for Experiment 3. For Experiments 4 and 5, they are important everywhere.

Possible sources of discrepancies are the following. As flows are at least unsteady in experiments, discrepancies could come from the fact that the code fails to predict this time-dependent flow regime. In the flow loop, the back flow behind the waterproof boxes could create pressure losses which may slow down the water flow and reduce therefore the channel flow rate. As explained previously, the residual fluctuations can reenter the channel and be amplified further downstream. Large velocity fluctuations which dissipate energy are measured at the channel inlet could result in developed boundary layers near the outlet. This is suggested by velocity profiles of Experiments 4 and 5 (Fig. 7) and there can be a change of flow regime for these modified Rayleigh numbers. This change can also be seen from the wall temperature distributions plotted in Fig. 8 against the channel height: in Experiments 4 and 5 wall temperature decreases in the downstream part. Note that the code provides a satisfactory prediction of the wall temperature for the two smallest modified Rayleigh numbers.

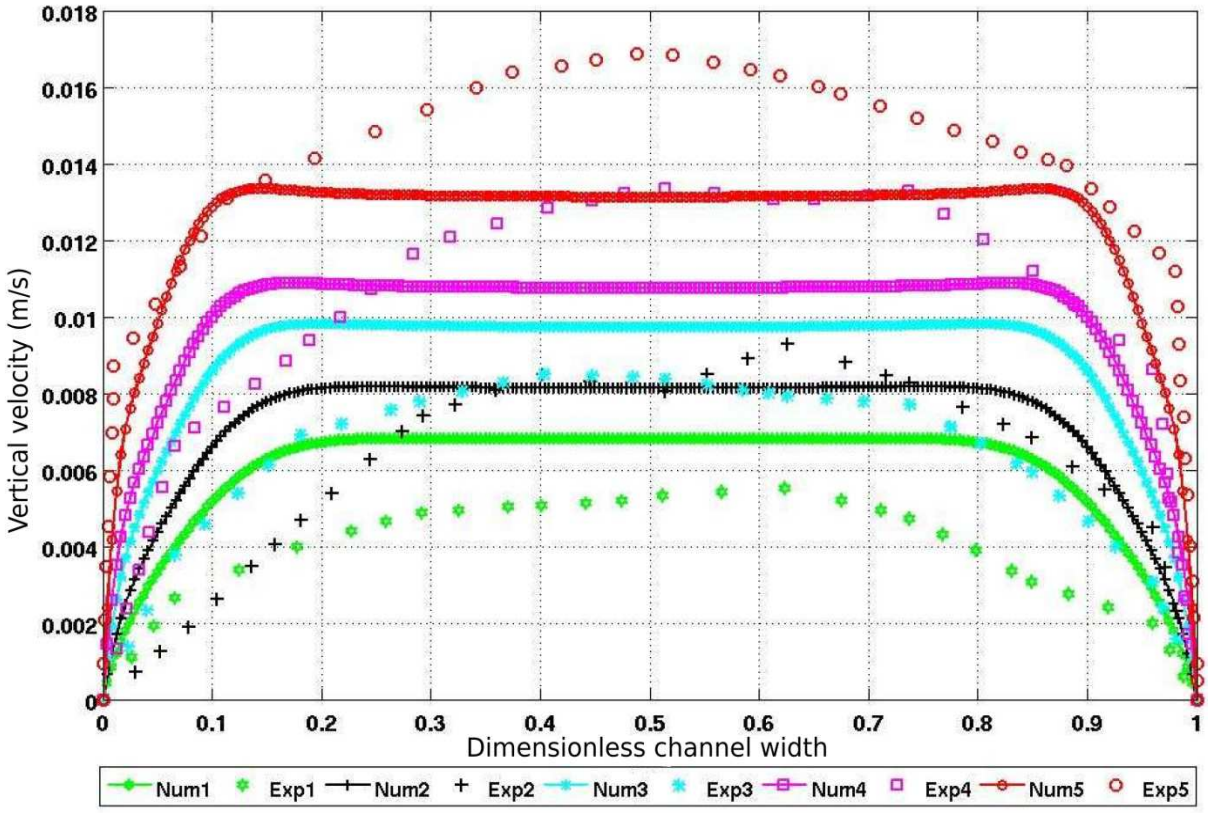

Fig. 6 Velocity distribution at the inlet ($y/L_h = 0.04$): comparison between numerical and experimental results.

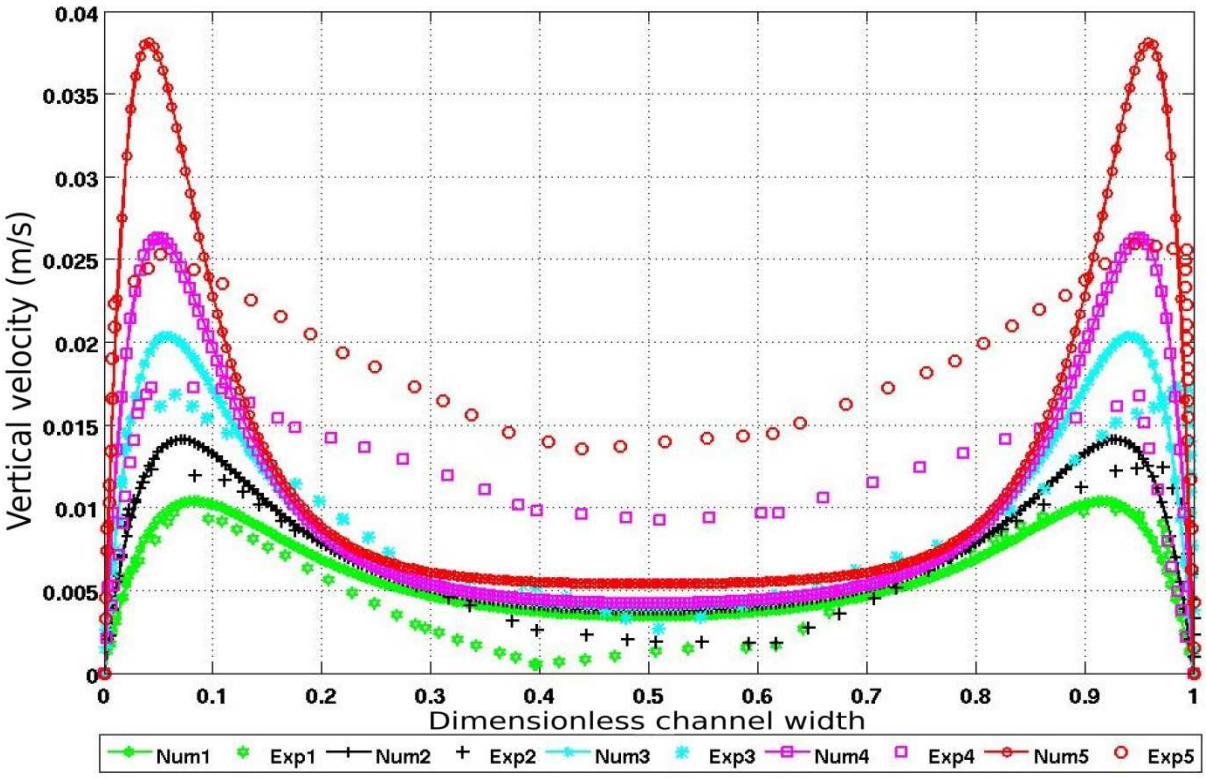

Fig. 7 Velocity distribution at the outlet ($y/L_h = 0.96$): comparison between numerical and experimental results.

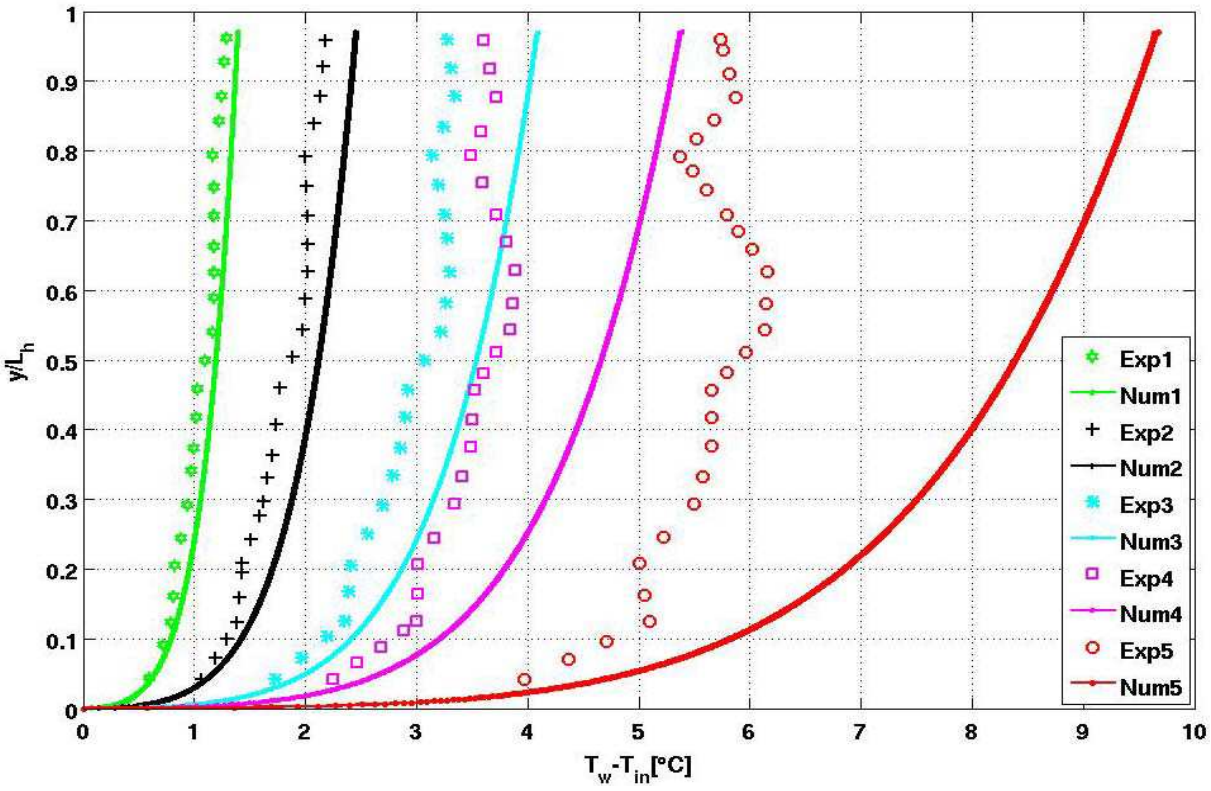

Fig. 8 Temperature differences between the right wall and the inlet versus dimensionless the heated channel height: comparison between numerical and experimental results.

6. Conclusions

The authors have presented a numerical code for studying natural convection in an open-ended channel. Finite difference scheme of second order in time and space was adopted to discretize the Navier-Stokes equations under the Boussinesq assumption. The inlet/outlet boundary conditions are based on Neumann boundary condition on vertical velocity and local Bernoulli for pressure at the channel inlet. The code was first validated with the GDR-AMETH numerical benchmark in the case of asymmetrical flux heating. The difference observed is of order of 2% and smaller than 5% (on maximum velocity). A grid convergence analysis was then carried out with $Ra_b^* = 100$ and aspect ratio of A = 5: the spatial scheme is globally of second order. Finally, numerical simulations were performed for a water-filled channel and results were confronted to experimental data for five modified Rayleigh numbers $Ra_b^* = 1.67 \times 10^6, 3.6 \times 10^6, 8.97 \times 10^6, 1.69 \times 10^7, 4.29 \times 10^7$ and aspect ratio $A \approx 14.5$. Comparison on flow rate, local Nusselt number, vertical velocity profiles (inlet/out) and wall temperature has been done between numerical and experimental data. For local Nusselt number and wall temperature good agreement is observed for the first two Ra_b^* while flow rates agree for the last two Ra_b^*. Nevertheless, discrepancy remains globally important for observed unsteady/turbulent flows in experiments and modeled steady regime in numerical study. Possible reasons for these discrepancies are discussed and further studies need to be carried out in order to improve both experimental and numerical approaches and understand the physical phenomena.

Acknowledgments

The authors would like to express their gratefulness to CLUSTER-Energy Région Rhône-Alpes for funding this investigation.

References

[1] W. Elenbaas, Heat dissipation of parallel plates by free convection, Physica 9 (1) (1942) 1-28.

[2] J.R. Bodoia, J.F. Osterle, The development of free convection between heated vertical plates, Trans. ASME 84 (1) (1962) 40-43.

[3] W. Aung, Fully developed laminar free convection between vertical plates, International Journal of Heat and Mass Transfer 15 (1972) 1577-1580.

[4] E. Sparrow, J. Gregg, Laminar free convection from a vertical plate with uniform surface heat flux, Trans. ASME 78 (2) (1956) 1-2.

[5] W. Aung, Developing laminar free convection between vertical flat plates with asymmetric heating, International Journal of Heat and Mass Transfer 15 (11) (1972) 2293-2308.

[6] T. Aihara, Effects of Inlet Boundary Conditions on Numerical Solutions of Free Convection between Vertical Parallel Plates, Tohoku University, Japan, 1973, pp. 1-27.

[7] A.M. Dalbert, F. Penot, J.L. Peube, Convection naturelle laminaire dans un canal vertical chauffe a flux constant, International Journal of Heat and Mass Transfer 24 (9) (1981) 1463-1473.

[8] O. Miyatake, H. Tanaka, T. Fujii, Natural convective heat transfer between vertical parallel plates: One plate with a uniform heat flux and the other thermally insulated, Heat Transfer-Japanese Research 4 (1973) 25-33.

[9] C. Kettleborough, Transient laminar free convection between heated vertical plates including entrance effects, International Journal of Heat and Mass Transfer 15 (5) (1972) 883-896.

[10] H. Nakamura, Y. Asako, T. Naitou, Heat transfer by free convection between two parallel flat plates, Numerical Heat Transfer 5 (1) (1982) 95-106.

[11] D. Naylor, J.M. Floryan, J. Tarasuk, A numerical study of developing free convection between isothermal vertical plates, J. Heat Transfer 113 (1991) 620-626.

[12] S. Ramanathan, R. Kumar, Correlations for natural convection between heated vertical plates, Trans. ASME 113 (1) (1991) 97-107.

[13] R.A. Wirtz, R.J. Stutzman, Experiments on free convection between vertical plates with symmetric heating, Journal of Heat Transfer 104 (3) (1982) 501-507.

[14] F. Bade, P. Haldenwang, High order scheme for thermally driven flows in an open channel, Computers & Fluids 27 (2) (1998) 273-290.

[15] A.G. Straatman, J.D. Tarasuk, J.M. Floryan, Heat transfer enhancement from a vertical, isothermal channel generated by the chimney effect, Journal of Heat Transfer 115 (2) (1993) 395-402.

[16] K.D. Kihm, J.H. Kim, L.S. Fletcher, Onset of flow reversal and penetration length of natural convective flow between isothermal vertical walls, Journal of Heat Transfer 117 (3) (1995) 776-779.

[17] B. Morrone, A. Campo, O. Manca, Optimum plate separation in vertical parallelplate channels for natural convective flows: Incorporation of large spaces at the channel extremes, International Journal of Heat and Mass Transfer 40 (5) (1997) 993-1000.

[18] A. Campo, O. Manca, B. Morrone, Numerical analysis of partially heated vertical parallel plates in natural convective cooling, Numerical Heat Transfer Part A, Applications 36 (2) (1999) 129-151.

[19] A. Auletta, O. Manca, Heat and fluid flow resulting from the chimney effect in a symmetrically heated vertical channel with adiabatic extensions, International Journal of Thermal Sciences 41 (12) (2002) 1101-1111.

[20] C.O. Olsson, Prediction of Nusselt number and flow rate of buoyancy driven flow between vertical parallel plates, Journal of Heat Transfer 126 (1) (2004) 97-104.

[21] C. Ménézo, M. Fossa, E. Leonardi, An experimental investigation of free cooling by natural convection of vertical surfaces for building integrated photovoltaic applications, in: THETA Conference, Cairo, Egypt, Jan. 3-6, 2007, pp. 125-131.

[22] M. Fossa, C. Ménézo, E. Leonardi, Experimental natural convection on vertical surfaces for building integrated photovoltaic applications, Experimental Thermal and Fluid Science 32 (4) (2008) 980-990.

[23] Q. Lu, S. Qiu, G. Su, W. Tian, Z. Ye, Experimental research on heat transfer of natural convection in vertical rectangular channels with large aspect ratio, Experimental Thermal and Fluid Science 34 (1) (2010) 73-80.

[24] E.M. Sparrow, P.A. Bahrami, Experiments on natural convection from vertical parallel plates with either open or closed edges, Journal of Heat Transfer 102 (2) (1980) 221-227.

[25] B.W. Webb, D.P. Hill, High Rayleigh number laminar natural convection in an asymmetrically heated vertical channel, Journal of Heat Transfer 111 (3) (1989) 649-656.

[26] S. Giroux-Julien, J. Vareilles, C. Ménézo, H. Pabiou, M. Fossa, E. Leonardi, Natural convection in non uniformly heated channel investigation--Application to photovoltaic façades, Computational Thermal Sciences 1 (2009) 231-258.

[27] G. Desrayaud, R. Bennacer, J.P. Caltagirone, E. Chenier, A. Joulin, N. Laaroussi, et al., Etude, Comparative numerical study thermoconvective flows in a vertical channel heated asymmetrically, in: 8th Inter—University Symposium Franco-Quebecers on thermodynamic systems, CIFQ2007/ART-06-14, May 28-30, 2007.

[28] F. Marcondes, C.R. Maliska, Treatment of the inlet boundary conditions in natural convection flows in open-ended channels, Numerical Heat Transfer Part B 35 (3) (1999) 317-345.

[29] J.M. Vanel, R. Peyret, P. Bontoux, A pseudo-spectral solution of vorticity-stream function equations using the influence matrix technique, Von Karman Inst. for Fluid Dynamics Computational Fluid Dynamics 1 (1986) 24-34.

[30] A.J. Chorin, A. Joel, The numerical solution of the Navier-Stokes equations for an incompressible fluid, Bulletin (New Series) of the American Mathematical Society 73 (6) (1967) 928-931.

[31] A. Joel, A.J. Chorin, A numerical method for solving incompressible viscous flow problems, Journal of Computational Physics 2 (1) (1967) 12-26.

[32] A. Zoubir, C. Daverat, S. Xin, S. Giroux-Julien, H. Pabiou, C. Ménézo, Numerical investigation for natural convection in a vertical channel: Comparison with experimental data, in: Proceedings of CHT-12, ICHMT International Symposium on Advances in Computational Heat Transfer, Bath, England, July 1-6, 2012.

[33] E.M. Sparrow, G.M. Chrysler, L.F. Azevedo, Observed flow reversals and measured-predicted Nusselt numbers for natural convection in a one-sided heated vertical channel, Journal of Heat Transfer 106 (2) (1984) 325-332.

[34] W. Aung, G. Worku, Developing flow and flow reversal in a vertical channel with asymmetric wall temperatures, Journal of Heat Transfer 108 (2) (1986) 299-304.

[35] P.J. Roache, K. Ghia, F. White, Editorial policy statement on the control of numerical accuracy, ASME Journal of Fluids Engineering 108 (1) (1986) 1-2.

[36] I. Celik, O. Karatekin, Numerical experiments on application of Richardson extrapolation with nonuniform grids, Journal of Fluids Engineering 119 (3) (1997) 584-590.

[37] F. Stern, R.V. Wilson, H.W. Coleman, E.G. Paterson, Verification and Validation of CFD Simulations, Iowa Institute of Hydraulic Research, University of Iowa, 1999.

[38] C.J. Roy, Grid convergence error analysis for mixed-order numerical schemes, AIAA Journal 41 (4) (2003) 595-604.